



Observations of the Ushant front displacements with MSG/SEVIRI derived sea surface temperature data



Clémence Chevallier^{a,*}, Steven Herbette^a, Louis Marié^a, Pierre Le Borgne^b, Anne Marsouin^b, Sonia Péré^b, Bruno Levier^c, Chris Reason^d

^a Laboratoire de Physique des Océans, UMR 6523, CNRS/IFREMER/IRD/UBO, 6 Avenue Le Gorgeu, 29200 Brest, France

^b Centre de Météorologie Spatiale, Avenue de Lorraine, 22307 Lannion, France

^c Mercator Ocean, Parc Technologique du Canal, 8-10 rue Hermès, 31520 Ramonville St Agne, France

^d University of Cape Town, Department of Oceanography, Rondebosch, South Africa

ARTICLE INFO

Article history:

Received 2 October 2012

Received in revised form 29 July 2013

Accepted 30 July 2013

Available online 2 November 2013

Keywords:

Tidal Front

High frequency Seviri SST

Front Detection

Tidal advection observed from satellite

Surface Currents Reconstruction

ABSTRACT

Hourly Sea Surface Temperature (SST) fields derived from the Spinning Enhanced Visible and Infra-Red Imager (SEVIRI) onboard Meteosat Second Generation (MSG) are frequently used in studies of the diurnal cycle of the ocean. In this article, we focus on high frequency SST variability induced by tidal currents in the Iroise Sea, west of Brittany (France). This region is known for its strong tidal currents that are responsible in summer for the generation of an intense thermal front, the Ushant front. We use hourly MSG/SEVIRI derived SST to compute the displacements of this front. In the northern part of the front, at 48.75°N, we show that the longitudinal displacements of the front on subdiurnal time scales can be explained by the Lagrangian advection induced by surface currents.

We also present maps of surface currents computed from hourly SEVIRI derived SST data using the Maximum Cross Correlation (MCC) method. Comparison of SEVIRI derived velocities with velocities obtained with high frequency (HF) radar measurements and a hindcast numerical simulation (Mercator Ocean) gives encouraging results in the northern part of the Ushant front, near the Ushant Island. Within that region, the mean bias of the SEVIRI velocities was below $0.12 \text{ m}\cdot\text{s}^{-1}$, with the standard deviation ranging from $0.26 \text{ m}\cdot\text{s}^{-1}$ during moderate tides to $0.49 \text{ m}\cdot\text{s}^{-1}$ during spring tides. Further offshore, where the surface thermal structures are weaker and the SST more homogeneous, currents derived using the MCC method were overestimated by $0.3 \text{ m}\cdot\text{s}^{-1}$ and showed larger error standard deviations.

© 2013 Elsevier Inc. All rights reserved.

1. Introduction

The Ushant thermal front is the main dynamical phenomenon of the Iroise Sea that lies off the coast of Western Brittany (France), and forms part of the Southern Celtic Sea. It is characterized by a strong temperature gradient that separates, in summer, warm and stratified offshore waters from cold and vertically mixed near-shore waters. This feature is observed from April–May to October, when the weakening of winds and increase of radiative fluxes allow a seasonal warming of the surface waters. Offshore, this warming is restricted to a roughly 30 m thick surface mixed layer bounded below by a seasonal thermocline. Inshore 3D turbulence sustained by bottom friction associated with strong tidal currents keeps the water column mixed over its full depth (roughly 100 m). Surface waters in the mixed area show a much reduced temperature seasonal cycle, and appear as a cool patch in satellite thermal imagery. Physical processes, related to the generation of tidal fronts, were first proposed by Simpson and Hunter (1974) for the Irish Sea

front. They showed that thermal tidal fronts were the result of a competition between two processes: stratification due to an increase of surface heat fluxes and vertical mixing due to the effect of bottom friction on tidal currents. Since then, there have been many in-situ observational programs to study the Ushant front (Le Boyer et al., 2009; Le Corre & Mariette, 1985; Szekely, Marié, Arduin, Sentchev, & Morel, in review; Szekely, Marié, Ferron, Cambon, & Morel, in review). Recently, high frequency radars have also been deployed on the coast to monitor surface currents (Arduin, Marié, Rasclé, Forget, & Roland, 2009; Sentchev, Forget, Barbin, & Yaremchuk, 2012). Additionally, several regional modeling studies have been carried out to study its dynamical behavior (Cambon, 2008; Mariette & Le Cann, 1985; Muller, Blanke, Dumas, & Mariette, 2010; Muller, Dumas, Blanke, & Mariette, 2007). The objective of the following work is to monitor the front displacements during a tidal cycle using maps of satellite derived sea surface temperature (SST).

Sequential infrared satellite images have been used for a long time to estimate ocean surface velocities (Crocker, Matthews, Emery, & Baldwin, 2007; Emery, Thomas, Collins, Crawford, & Mackas, 1986; Tokmakian, Strub, & McClean-Padman, 1990). These studies have used polar orbiter

* Corresponding author. Tel.: +33 298016218; fax: +33 298224496.

E-mail address: Clemence.Chevallier@univ-brest.fr (C. Chevallier).

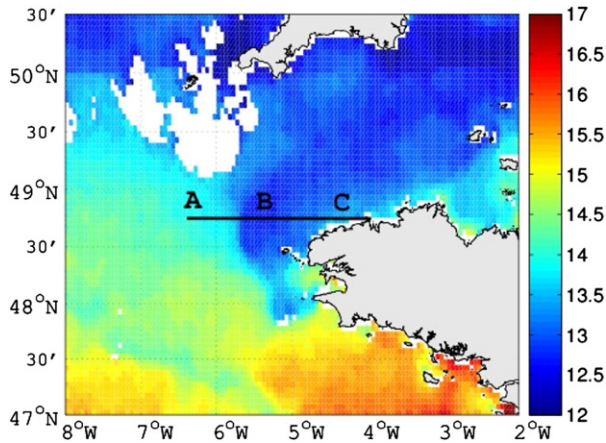


Fig. 1. SEVIRI derived SST field ($^{\circ}\text{C}$) on May 30th, 2009 at 03:00 UTC with location of the section (black line) crossing the front along 48.75°N . A, B and C represent 3 different water masses in the vicinity of the Ushant front: respectively the warm and stratified waters, the cold and mixed waters and the coastal waters.

derived thermal fields, with 12 hour sampling. In order to monitor rapidly varying tidal surface currents, higher frequency sampling is needed. Thus, we used the high frequency SST data derived from the Spinning Enhanced Visible and Infra-Red Imager (SEVIRI) onboard Meteosat Second Generation (MSG). Hourly SEVIRI derived SST fields are produced by the EUMETSAT Ocean & Sea Ice Satellite Application Facility (OSI-SAF). To date, the high frequency SST images provided by SEVIRI have been used primarily for diurnal warming studies (Gentemann, Minnett, Le Borgne, & Merchant, 2008; Le Borgne, Legendre, & Péré, 2012; Merchant et al., 2008). Our objective, in this contribution, is to show

the abilities and limitations of geostationary satellite imagery to study the high frequency variability and surface velocities associated with the Ushant front. To our knowledge, this is the first attempt to take advantage of the high frequency sampling provided by SEVIRI to study such dynamical processes.

Section 2 presents the satellite, HF radar and model datasets used in this study. Section 3 demonstrates that front displacements deduced from SEVIRI SST images relate to advection by surface currents. In Section 4, we use hourly SEVIRI SST data to compute surface velocities using a Maximum Cross Correlation technique (MCC, Emery et al., 1986). These SEVIRI derived velocities are compared to high frequency radar measurements and ocean model outputs (Section 5). Finally, in Section 6 we conclude and briefly present perspectives for future work.

2. Data

Our region of interest (47°N – 50°N , 8°W – 2°W) is located off the French coast of Western Brittany (Fig. 1). Cloud cover is a common limiting factor inherent to the use of infrared satellite data. We focus on a period for which we were able to extract a time series of successive hourly cloud free SST images for almost six days, between May 29th and June 3rd 2009. The period was characterized by moderate tides. Being quite early in the summer season, it also corresponded to a relatively mild cross-front temperature difference on the order of 1.5°C compared to the 5°C temperature differences commonly observed in late summer across the Ushant front.

Our analysis was mainly based on SEVIRI derived SST (EUMETSAT, 2006). SEVIRI observes a given location with a constant viewing geometry every 15 min, with a 5 to 6 km ground resolution over Brittany. We used the experimental hourly SST fields made available on a 0.05° regular grid by OSI-SAF at Centre de Météorologie Spatiale (CMS) in Lannion (France). The SEVIRI derived velocity fields were compared with the

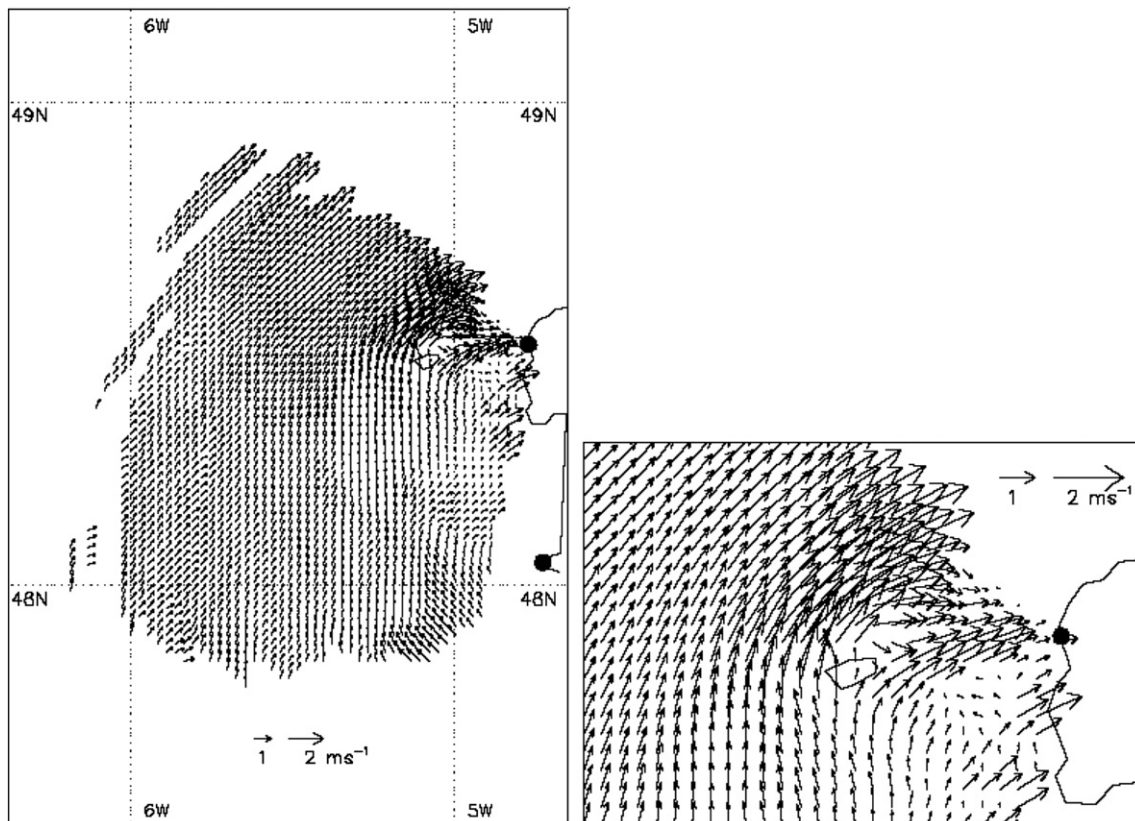


Fig. 2. Example of a surface velocity field derived from high frequency radars on May 30th, 2009 at 07:30 UTC. The left figure shows the whole area on its original grid, the right figure zooms on the area around the Ushant Island. The system includes two radar stations located on the West Brittany coast (filled black circles).

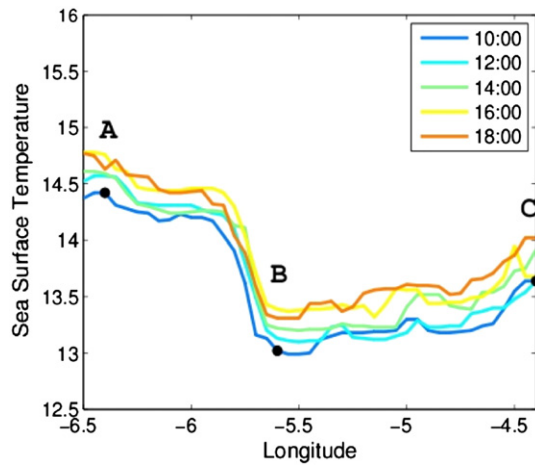


Fig. 3. SST ($^{\circ}\text{C}$) section along 48.75°N from 6.5°W till 4.5°W on June 1st, 2009. The colored curves correspond to different time of the day, from 10:00 UTC to 18:00 UTC.

ones resulting from the Ireland Biscay Iberia (IBI) Regional Mercator Ocean model. The IBI SST and velocities came from a test run that was carried out with a 2 km horizontal resolution over our domain and period of interest (Cailleau, Chanut, Levier, Maraldi, & Reffray, 2010). The IBI surface outputs, representative of the first meter of the ocean, were then remapped onto the SEVIRI grid. Surface current measurements provided by Service Hydrographique et Océanographique de la Marine (SHOM) with a time resolution of 10 min were also used for validation. These measurements were obtained using a two-site WERA HF radar system (Gurgel, Antonischki, Essen, & Schlick, 1999; Gurgel, Essen, & Kingsley, 1999) located along the Western Brittany coast. The stations' location and the area covered by the system are shown in Fig. 2. A description of the set-up can be found in Arduin et al. (2009). Raw HF radar measurements are affected by a bias related to the wave-induced Stokes drift. Corrections for this effect were applied for the comparison presented in Section 3, as discussed in Arduin et al. (2012, 2009).

3. Front displacement

Using thermal imagery, we analyzed the shape and position of the Ushant front over the study period, and noticed that the intensity and orientation of the northern part of the front, between 48.5°N and 49°N , given by the magnitude and angle of the SST gradient, were almost constant. Within that zone, the front was characterized by a mostly north–south orientation, and very cold SST on its onshore side, which led to a relatively strong zonal gradient. Therefore, east to west displacements of the front within that zone were easier to observe than anywhere else along the front, and we decided to focus our study on a longitudinal section at 48.75°N (Fig. 1).

Fig. 3 shows the SST cross-front profiles along that section between 10:00 UTC and 18:00 UTC on June 1st 2009. A strong SST gradient (up to $0.05^{\circ}\text{C}\cdot\text{km}^{-1}$) is evident throughout this period. It marks the separation between the cold onshore vertically mixed waters and the offshore stratified waters. The dark blue curve (the coldest) is the morning SST profile whereas the red and yellow curves correspond to afternoon SST profiles. Diurnal warming of nearly 0.5°C occurs both in the stratified waters (A) and in the mixed waters (B). This was an unexpected feature requiring further study, which is beyond the scope of this work. Nevertheless, for the present study it should be noted that diurnal warming did not have a large effect on the local SST gradient related to the tidal front.

In order to track the front in time, we needed to define accurately the position of the Ushant front in our SST images. Ideally, this position should correspond to the largest magnitude of the SST gradient. Nevertheless, in practice, gradients deduced from non-filtered SST images show spurious features that do not correspond to real physical phenomena. Many automated algorithms have already been developed to detect frontal structures in SST images. Two main groups of algorithms can be distinguished; those based on first or second order spatial derivative of the SST data (Canny, 1986) and those based on the fact that edges found in the Ocean SST usually result from two separate water masses (Cayula & Cornillon, 1992). For the latter, histogram analysis is first used to characterize the presence of several water masses. Because the purpose of this study was not to develop an automated algorithm capable of detecting the front at every time step, we constructed an algorithm based on a simple gradient method. First, the SST image was filtered using a 3×3 pixel median filter. The median filtered SST image was

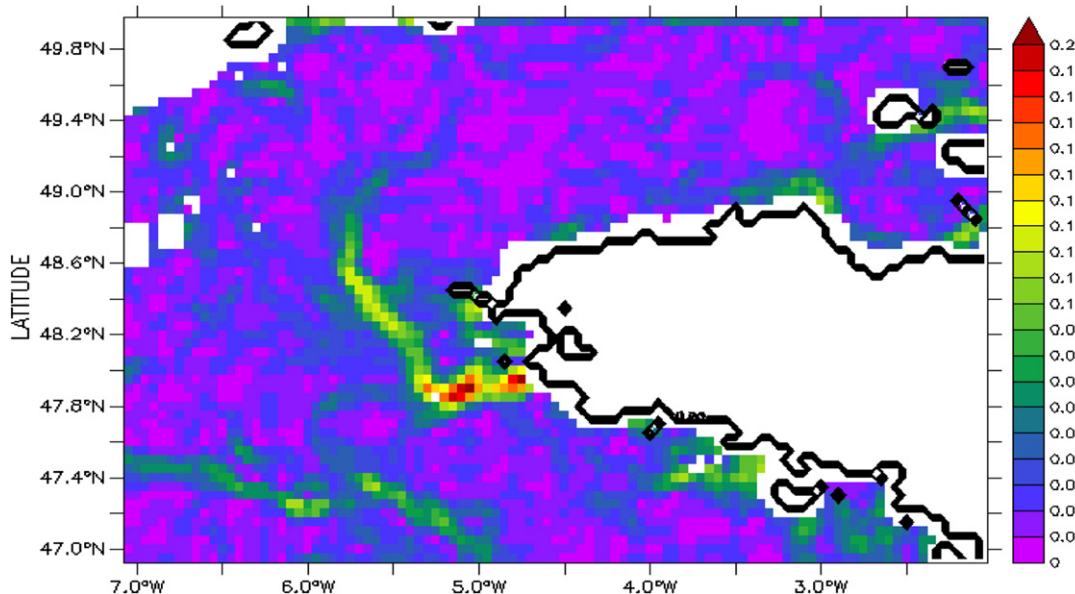


Fig. 4. Gradient values in ($^{\circ}\text{C}\cdot\text{km}^{-1}$) derived by applying a Sobel filter to the SST fields at 18:00 on May 30th, 2009.

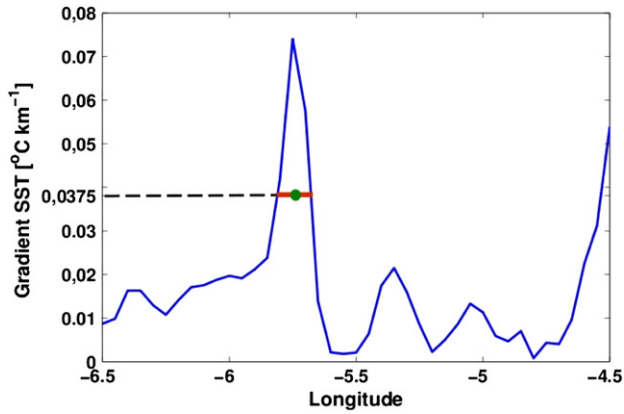


Fig. 5. Gradient values in ($^{\circ}\text{C}\cdot\text{km}^{-1}$) along the 48.75°N section at 17:00 UTC on June 1st, 2009. The red segment denotes the empirical threshold of $0.0375^{\circ}\text{C}\cdot\text{km}^{-1}$. The green dot is the middle of this segment. The latter was found to best represent the front location.

then convolved with a Sobel filter to obtain the magnitude and direction of the SST gradient. A horizontal map of the SST gradient for May 30th, 2009 at 18:00 UTC is shown in Fig. 4. The cross-frontal profile of the SST gradient, at 48.75°N for June 1st 2009 at 17:00 UTC, is plotted in Fig. 5. A large amplitude broad peak at approximately 5.75°W corresponds to the frontal zone separating cold inshore surface waters from warm offshore surface waters. Fig. 6 presents the collection of surface temperature gradient profiles corresponding to the zonal temperature profiles shown in Fig. 3. Each profile clearly displays a strong peak, whose shape, maximum height and position vary with time. These variations may be linked to several physical processes related to:

- i) Water mass advection by surface currents. Comparison with HF radar measurements (see below) showed that this effect was dominant. In Section 4, we exploited this property to extract surface velocity information from the SST data. However, Fig. 6 shows that the displacement of the peak was only marginally resolved in the SEVIRI SST fields, making the use of a sub-pixel front tracking method necessary.
- ii) Heterogeneities in the cross-front component of the currents. The latter may change the peak maximum height. A convergence of the across-front component of the currents tends for instance to draw isotherms closer, hence increasing the maximum gradient value. This effect is quite relevant in the present situation, in

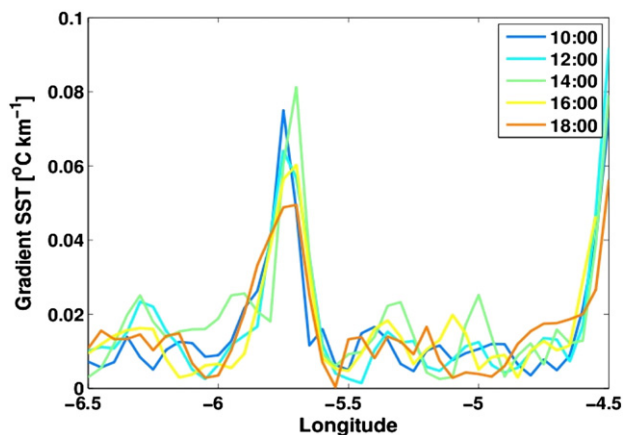


Fig. 6. Gradient values in ($^{\circ}\text{C}\cdot\text{km}^{-1}$) along the 48.75°N section on June 1st, 2009. The colored curves correspond to different time of the day, from 10:00 UTC to 18:00 UTC.

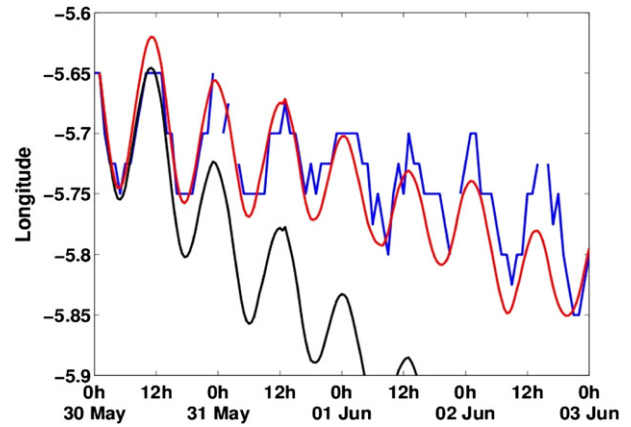


Fig. 7. Front location derived from SEVIRI SST (blue) compared to the corresponding surface advection calculated from raw HF radar measurements (black) and the data corrected for the surface Stokes drift bias (red).

which the close proximity of the coast and islands might induce a distortion of the strong tidal currents.

- iii) Modulation of air/sea heat fluxes due to the different SST values on either sides of the front. For the study period, air temperature measured at 48.5°N , 5.8°W was marginally higher than SST in the cool region. This situation may induce larger sensible heat fluxes over the cool region, and in some degree, some ocean surface cooling in the stratified zone. This might explain the slightly reduced diurnal warming observed west of the front in the SST profiles of Fig. 3. This effect, which results in a decrease of the cross-front temperature difference, may induce a slight lowering of the gradient peak value.
- iv) Cross-frontal variation of the vertical mixing efficiency. It is a classical expectation that micro-scale mixing should be more active on the onshore side of the front than offshore. This should lead to a smaller degree of diurnal warming on the cool side, the heat injected at the surface by solar radiation being more rapidly dispersed downwards. The SST profiles of Fig. 3 show that this is however clearly not the case, at least for the period under study. In fact, direct microstructure turbulence measurements performed during the FromVvar 2009 cruise have

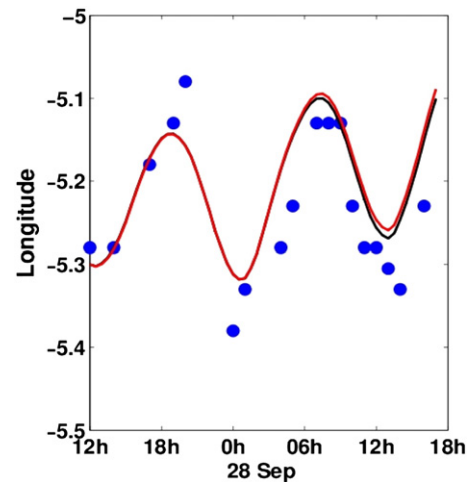


Fig. 8. Front location derived from SEVIRI SST (blue dots) compared to the corresponding surface advection calculated from raw HF radar measurements (black) and the data corrected for the surface Stokes drift (red), during a spring tide period: September 27th–28th, 2011.

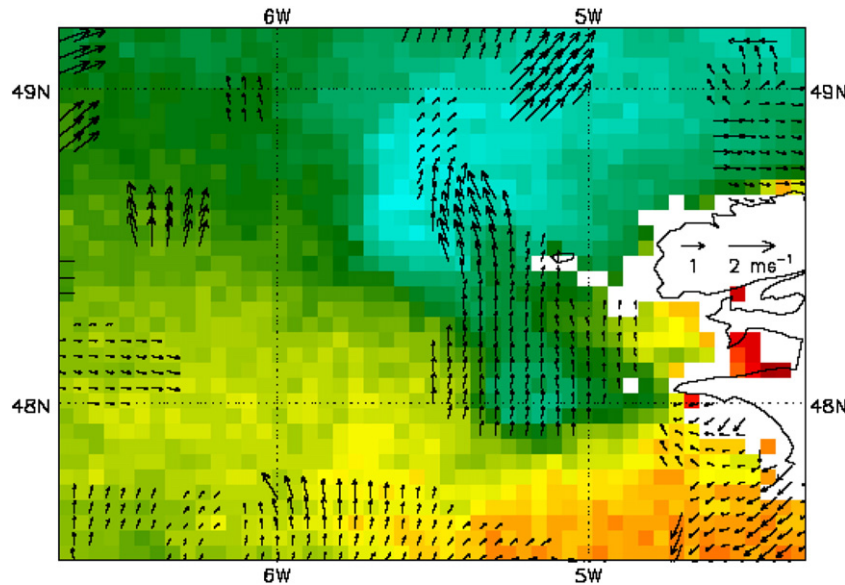


Fig. 9. SEVIRI SST derived velocity vectors on May 30th, 2009, from 05:00 to 08:00 UTC, superimposed on the 08:00 UTC SST field.

shown the modulation of micro-scale mixing by this front to be marginal. These results are discussed in Szekely, Marié, Ferron, et al. (in review).

- v) Increased horizontal mixing due to a variety of (sub-)meso-scale instabilities resulting from the sharp cross-front temperature difference. These instabilities manifest themselves in the form of meanders of the front (see the satellite images in Le Boyer et al., 2009; Muller et al., 2010), which tends to lower the temperature gradient. However, these effects are expected to evolve on longer, at least diurnal, time-scales than the variability studied in this article.

As mentioned in the previous paragraph, Fig. 6 shows that a sub-pixel accurate method must be used to track the front position, which is only marginally resolved in the SEVIRI data. We empirically estimated the front position as the middle of a segment defined by the $0.0375\text{ }^{\circ}\text{C}\cdot\text{km}^{-1}$ threshold in the SST gradient cross-frontal profile (middle of the red segment in Fig. 5). We used this method to follow the front position along the 48.75°N section over several days at hourly intervals. Fig. 7 shows a comparison between displacements of the front, as identified in SEVIRI SST images, and displacements inferred from time integration of HF radar derived surface velocities. The objective of this step was to determine if the displacements of the front observed in SEVIRI SST images were due to physical processes as opposed to processing issues. For this comparison, in order to reduce the impact of data gaps, HF radar measurements were averaged over a rectangular box bounded by the 5.4°W and 5.25°W parallels and the 48.55°N and 48.7°N latitudes. Integration in time was performed using the raw data (black line), and the data corrected for the surface Stokes drift bias, as discussed in Ardhuin et al. (2009) (red line). All curves share a conspicuous semi-diurnal component, in agreement with the tidal current characteristics of the area. The estimates of the tidal displacement amplitude agree closely and are of the order of 0.1° longitude, approximately 7.3 km. The slow drift of the frontal position with time is not uncommon, and can be due to many factors such as slow advection by rectified tidal currents or wind-forced Ekman drift. In fact, wind data from the Ushant lighthouse, provided by Météo-France over that period, revealed a dominant East/North-East direction. The moderate (5–10 m/s) wind over the period induces a noticeable contamination of the raw HF radar data by the surface wave Stokes drift, and to a strong over-estimate of the residual movement of the front (black curve). Correcting this effect leads to a very good match between

completely independent measurement techniques. Finally, another interesting point is that the close match between frontal motion and water particle displacements clearly points to the dominant impact of advection, with respect to diabatic heating/cooling, on sea surface temperature gradients at these time scales. Fig. 8 shows the results of a similar study for a spring tide case (September 2011). The clear-sky period is shorter than for the May 2009 case but similar features can be observed, which confirms the previous results. The origin and characteristics of surface currents in the Iroise Sea are discussed in detail in the work of Sentchev et al. (2012) and Szekely, Marié, Ardhuin, et al. (in review). Tidal currents account for most of the observed surface currents and can be considered to be spatially homogeneous over the cross-frontal length scale. Surface current anomalies in thermal wind balance with the density front are too weak to generate a significant distortion of the front on tidal time scales. This suggests a nearly passive and conservative behavior of sea surface temperature gradients on daily time scales in the region. Hence, the latter can be used as near-Lagrangian water mass markers. We thus decided to go one step further and used the SST images to derive surface velocity vectors.

4. Estimation of surface velocity fields using SST data

Previous studies (Crocker et al., 2007; Emery et al., 1986; Tokmakan et al., 1990), dealing with velocity vectors estimated from SST images, were based on the Maximum Cross-Correlation (MCC) method. This method, which consists of the following steps, was applied to time sequences of SEVIRI SST images at 0.05° resolution (approximately 5.5 km for the meridional grid step).

- a) SST images were considered in pairs. For each pixel in the reference image of a pair, an 11×11 box, centered on the pixel, was defined. This box was referred to as the reference box. Similar boxes were defined for each pixel in the second image of the pair. For each cloud free pixel in the reference image, correlations were calculated between the SST data of the associated box and the SST values in boxes in the second image that are within a few pixels of the reference box. The position at which the correlation was maximum defined the optimal displacement, expressed in line and pixel numbers of the SST image.
- b) Validity tests were carried out to eliminate non-significant optimal displacements. Only optimal displacements corresponding

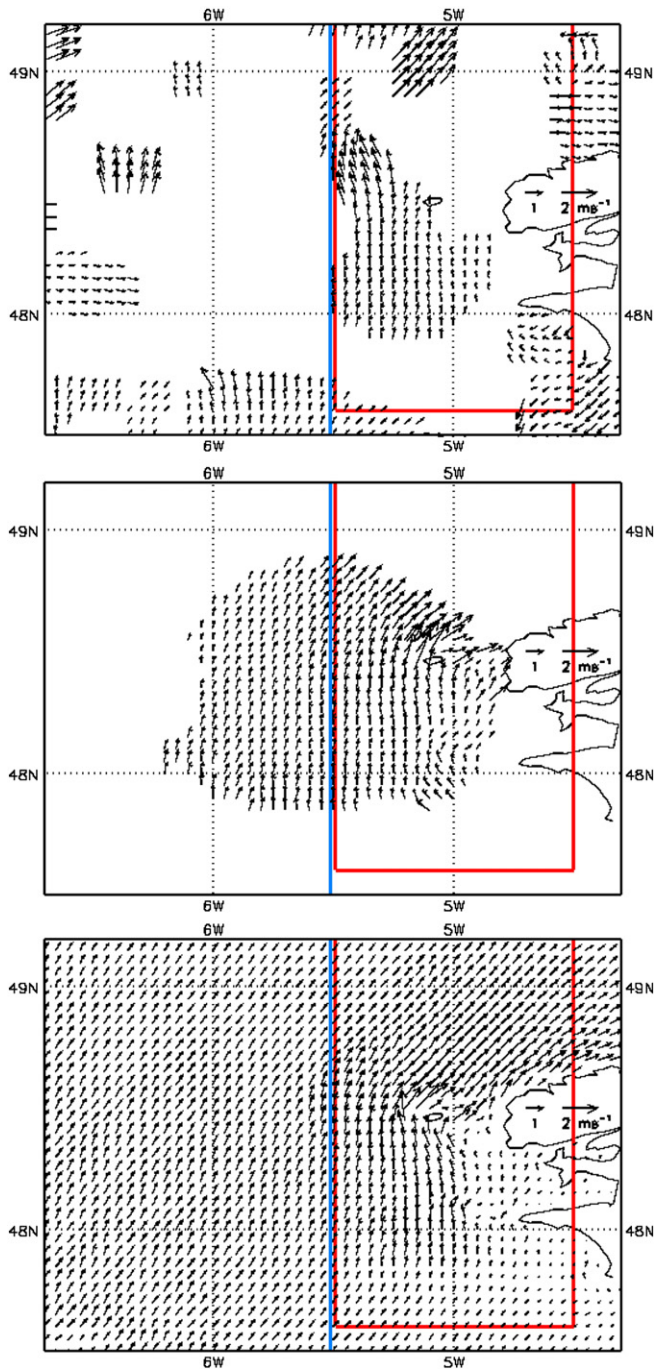


Fig. 10. Velocity vectors on May 30th, 2009, from 05:00 to 08:00 UTC, from 3 datasets: SEVIRI SST (top), HR radar measurements (middle) and IBI model outputs (bottom). The Ushant area is limited by the red lines, the offshore area is west of the blue line.

to correlations greater than 0.75 and more than 0.05 above the correlation assuming no motion (without moving the box) were retained. We also required a minimum number of cloud free SST pixels in each box. Additionally, the difference between the mean SST of the optimal and reference box had to be less than 0.3 °C. These threshold values were chosen empirically.

- c) When an optimal displacement was considered as valid, an attempt was made to obtain an improved displacement value at sub-pixel resolution. A 2nd order polynomial was fit to the correlation values on a 3×3 box centered on the optimal displacement position. If this adjustment succeeded, the position at which the polynomial was

maximum defined a second optimal displacement, expressed in real line and pixel numbers, which replaced the previous optimal values.

- d) The displacement vectors were then converted into velocity vectors based on the elapsed time between the two SST images and the pixel separation in the two directions.

For our domain of interest, we used a 3-hour interval between SST fields to obtain displacement values observable at 0.05° resolution. Displacements based on image pairs separated by 1 h were too small considering the resolution of the SEVIRI SST data. Eleven pixel square boxes, i.e. 55 km, were chosen for the MCC method as they showed, on average, better correlations and more spatially consistent velocity fields.

Fig. 9 shows an example of SEVIRI derived velocity vectors superimposed on the second SST field of the pair. Even for this rather clear sky image pair, velocity vectors were patchy with velocity retrievals failing the validity tests at many clear pixel locations.

5. Validation of SEVIRI derived surface velocities

We compared the SEVIRI derived velocity vectors with two surface current datasets: IBI model (Mercator Ocean) output available hourly and raw HF radar measurements available every 10 min. The surface currents were averaged over 3 h to be consistent with SEVIRI surface currents. Fig. 10 shows the SEVIRI, IBI, and radar velocity vectors for May 30th 2009 at 06:30 UTC. Good agreement was found in the eastern part of the region, near the Ushant Island. Further offshore, SEVIRI velocity vectors proved to be erroneous. Similar results were found for all subsequent times at which we were able to derive surface currents from the SEVIRI data (not shown). All three (SEVIRI, IBI and radar) surface velocity fields had a correlation length scale much larger than the cross-frontal scale, except in the immediate vicinity of the islands and coastline, and did not seem affected by the presence of the front. As mentioned above, this was expected, as the tidal component of surface current, which is correlated on large spatial scales, overwhelms the geostrophic current anomaly associated with the density front.

Statistics for the comparison of IBI and SEVIRI velocities and for the HF radar and SEVIRI velocities were calculated for the two areas, one near the Ushant island and the other further offshore, for two time periods, one corresponding to moderate tides and the other to spring tides. These statistics are presented in Table 1. When compared to IBI and HF radar velocities, SEVIRI velocities in the Ushant area show low mean errors and high error standard deviations, about $0.25 \text{ m}\cdot\text{s}^{-1}$ in moderate tide and $0.49 \text{ m}\cdot\text{s}^{-1}$ in spring tide. Further offshore, SEVIRI derived velocity vectors match neither the radar measurements nor the model output: they show high mean errors, about $0.3 \text{ m}\cdot\text{s}^{-1}$ for the period of moderate and spring tides. Although tidal surface currents are strong over the whole region, the off-shore surface waters have a much more homogeneous SST, which makes it more difficult for the MCC algorithm to track isolated features. Additionally, off-shore-SSTs are more consistent in time, which explains why correlation of SST patterns between two successive images was high enough not to be rejected by the validation procedure. For the period and area studied, statistics differentiating the X and Y velocity components (not shown) does not provide any additional information.

6. Conclusions

Observations of the Ushant front with SEVIRI/MSG SST fields during a moderate tide period (May, 29th–June, 3rd 2009), at one hour intervals, showed that the displacement of the thermal front was identifiable and was driven by surface currents. The high frequency sampling of the SEVIRI SST also showed that diurnal warming could be significant in the area, both for stratified off-shore and vertically mixed on-shore waters, at least in the northern part of the front along 48.75°N. Nevertheless, it is interesting to note that the cross frontal SST gradient was only

Table 1

Comparison of velocities derived from SEVIRI SST imagery, IBI numerical model, and HF radar surface data. In column 1, “moderate tides” correspond to the period extending from 2009-05-30 at 00:00 UTC to 23:00 UTC, and “spring tides” to the period extending from 2011-09-27 at 14:00 UTC to 2011-09-28 at 14:00 UTC. Column 2 gives the reference dataset name. “#cases” is the number of cases (having a valid velocity vector in the 3 datasets), “bias” the mean error, “stdev” the error standard deviation and “mean” the mean velocity of the reference dataset.

		Ushant area 47.6 N 49.3 N 5.5 W 4.5 W				Offshore area 47 N 50 N 7 W 5.5 W			
		# cases	Bias $m \cdot s^{-1}$	Stdev $m \cdot s^{-1}$	Mean $m \cdot s^{-1}$	# cases	Bias $m \cdot s^{-1}$	Stdev $m \cdot s^{-1}$	Mean $m \cdot s^{-1}$
Moderate tides	IBI	957	-0.02	0.23	0.57	681	0.35	0.30	0.43
	Radar	957	0.01	0.26	0.55	681	0.27	0.36	0.51
Spring tides	IBI	2297	-0.11	0.48	0.85	1526	0.30	0.49	0.74

marginally affected by diurnal warming. All together, these results tend to show that, in the region of interest, the time scale related to vertical mixing processes induced by bottom friction is larger than the advection time scale due to the existence of strong tidal currents.

Having gained some confidence in our ability to track the front, we used the SEVIRI/MSG SST data to compute surface velocity vectors using the MCC. Surface currents, at 3 h intervals, were obtained for a spring tide period (September 2011) and a moderate tide period (May–June 2009).

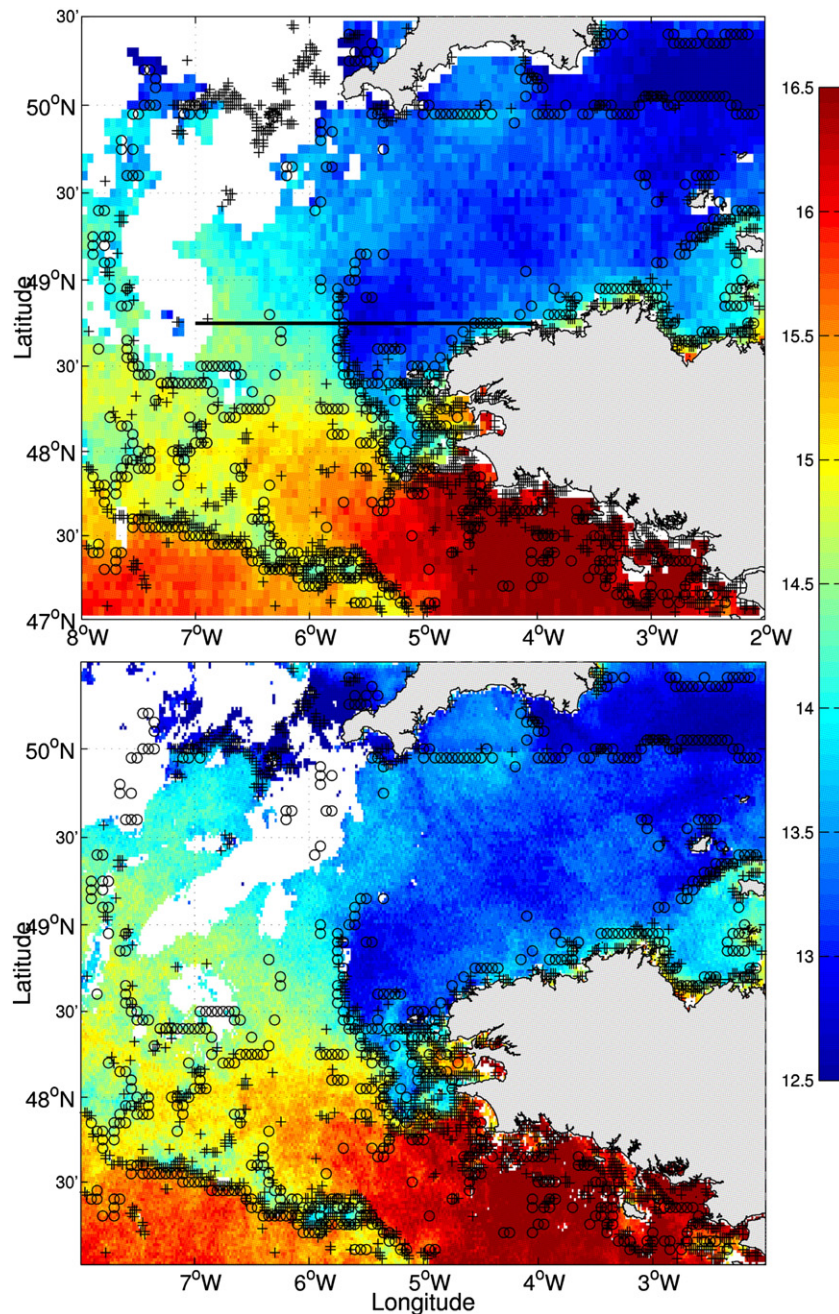


Fig. 11. SST on May 30th, 2009 at 21:00 UTC from SEVIRI (top) and Metop (bottom). Position of the Ushant front, deduced using the gradient-based algorithm of Canny (1986), from the SEVIRI image at 6 km resolution (circles) and the METOP image at 2 km resolution (crosses) coincide.

SEVIRI derived velocity vectors were compared to surface currents from HF radar measurements and IBI model (Mercator Ocean) outputs. The success of the method was marginal: it performed reasonably well in the Ushant front area but failed in the rather homogeneous offshore area. The algorithm should be improved to increase the accuracy of our velocities and eliminate non-significant values in areas of homogeneous surface waters. The present analysis should be seen as a first attempt in using SEVIRI SST to determine surface velocities. With the capabilities and limitations of the method in mind, this study could be readily extended to other periods in the SEVIRI time series. The University of Rhode Island (URI), in collaboration with MF/CMS has prepared a suite of SST front and gradient datasets based on the full time series of SEVIRI derived SST fields, dedicated to such studies. These datasets are available on the URI fronts/gradient web site: <http://www.sstfronts.org>.

Our analysis of the front displacements and short time variability was only performed on the northern part of the Ushant front along 48.75°N, mainly because it was easy to track the front along that line. The use of the Canny (1986) edge detection algorithm on SST images has been used successfully in coastal areas (Oram, Mc Williams, & Stolzenbach, 2008). It could be applied in the Ushant front area to track the entire front over the domain (Fig. 11). Some spatial variability may be found in the processes (advection versus horizontal or vertical mixing) governing the front positions. Additionally, our analysis should be carried out over different time periods to gain in robustness and develop some knowledge on the intra-seasonal time variability of the Ushant front. This is obviously a difficult task considering the significant data gaps in the coastal waters off Western Brittany due to cloud cover.

The diurnal warming that was observed both in the stratified and vertically mixed region of the Ushant front would also require further work to understand why it reached a similar amplitude in both regions. Some field work was dedicated to this question in September 2009 and 2011.

Acknowledgments

The data from the EUMETSAT Satellite Application Facility on Ocean and Sea Ice is accessible through the SAF's homepage: <http://www.osi-saf.org>. We thank the Service Hydrographique et Océanographique de la Marine (SHOM) for giving us access to the HF radar data. We thank Fabrice Arduin for making available the HF radar Stokes drift bias correction data. We thank our anonymous reviewers for helpful and thoughtful suggestions for improving this article. This work is part of the EPIGRAM project funded by CNRS (LEFE/IMAGO) and ANR (grant ANR-08-BLAN-0330-01).

References

Arduin, F., Dumas, F., Bennis, A. -C., Roland, A., Sentchev, A., Forget, P., et al. (2012). Numerical wave modeling in conditions with strong currents: Dissipation, refraction and relative wind. *Journal of Physical Oceanography*, 42, 2101–2120.

- Arduin, F., Marié, L., Rasclé, N., Forget, P., & Roland, A. (2009). Observation and estimation of Lagrangian, Stokes and Eulerian currents induced by wind and waves at the sea surface. *Journal of Physical Oceanography*, 39, 2820–2838.
- Cailleau, S., Chanut, J., Levier, B., Maraldi, C., & Reffray, G. (October 39). *The new regional generation of Mercator Ocean system in the Iberian Biscay Irish (IBI) area*. Mercator Ocean Quarterly Newsletter, 5–15.
- Cambon, G. (2008). *Etude numérique de la mer d'Iroise: Dynamique, Variabilité du front d'Ouessant et Evaluation des échanges cross-frontaux*. PhD thesis. : Université de Bretagne Occidentale.
- Canny, J. (1986). A computational approach to edge detection. *IEEE Transactions on Pattern Analysis and Machine Intelligence, PAMI-8(7)*, 679–698.
- Cayula, J. -F., & Cornillon, P. (1992). Edge detection algorithm for SST images. *Journal of Atmospheric and Oceanic Technology*, 9, 67–80.
- Crocker, R. I., Matthews, D. K., Emery, W. J., & Baldwin, D. G. (2007). Computing coastal ocean surface currents from infrared and ocean color satellite imagery. *IEEE Transactions on Geoscience and Remote Sensing*, 45, 435–447. <http://dx.doi.org/10.1109/TGRS.2006.883461>.
- Emery, W. J., Thomas, A. C., Collins, M. J., Crawford, W. R., & Mackas, D. L. (1986). An objective method for computing advective surface velocities from sequential satellite images. *Journal of Geophysical Research*, 91(C11), 12 865–12 878.
- EUMETSAT (2006). Atlantic sea surface temperature product manual. http://www.osi-saf.org/biblio/docs/ss1_pmatlsst_1_6.pdf [available online]
- Gentemann, C. L., Minnett, P. J., Le Borgne, P., & Merchant, C. J. (2008). Multi-satellite measurements of large diurnal warming events. *Geophysical Research Letters*, 35, L22602. <http://dx.doi.org/10.1029/2008GL035730>.
- Gurgel, K. -W., Antonischki, G., Essen, H. -H., & Schlick, T. (1999). Wellen radar (WERA): A new ground-wave HF radar for ocean remote sensing. *Coastal Engineering*, 37(3), 219–234.
- Gurgel, K. -W., Essen, H. -H., & Kingsley, S. P. (1999). High-frequency radars: Physical limitations and recent developments. *Coastal Engineering*, 37(3), 201–218.
- Le Borgne, P., Legendre, G., & Péré, S. (2012). Comparison of MSG/SEVIRI and drifting buoy diurnal warming estimates. *Remote Sensing of Environment*, 124, 622–626.
- Le Boyer, A., Cambon, G., Daniault, N., Herbette, S., Le Cann, B., Marié, L., et al. (2009). Observations of the Ushant tidal front in September 2007. *Continental Shelf Research*, 29, 1026–1037.
- Le Corre, P., & Mariette, V. (1985). Le front thermique d'Ouessant en août et septembre 1982, Campagne SATIR–DYNATLANT. In IFREMER, GREPMA-CNRS (Ed.), *Campagnes Océanographiques Françaises, Vol n°1*. (pp. 369).
- Mariette, V., & Le Cann, B. (1985). Simulation of the formation of Ushant thermal front. *Continental Shelf Research*, 4(6), 637–660.
- Merchant, C. J., Filipiak, M. J., Le Borgne, P., Roquet, H., Autret, E., Piolle, J. -F., et al. (2008). Diurnal warm-layer events in the western Mediterranean and European shelf seas. *Geophysical Research Letters*, 35, L04601. <http://dx.doi.org/10.1029/2007GL03071>.
- Muller, H., Blanke, B., Dumas, F., & Mariette, V. (2010). Identification of typical scenarios for the surface Lagrangian circulation in the Iroise sea. *Journal of Geophysical Research*, 115, C07008 [N.].
- Muller, H., Dumas, F., Blanke, B., & Mariette, V. (2007). High resolution atmospheric forcing for regional oceanic model: The Iroise Sea. *Ocean Dynamics*, 57, 375–400.
- Oram, J. J., Mc Williams, J. C., & Stolzenbach, K. D. (2008). Gradient-based edge detection and feature classification of sea-surface images of the Southern California Bight. *Remote Sensing of Environment*, 112, 2397–2415.
- Sentchev, A., Forget, P., Barbin, Y., & Yaremchuk, M. (2012). Surface circulation in the Iroise Sea (W. Brittany) from high resolution HF radar mapping. *Journal of Marine Systems*, 109, 153–168.
- Simpson, J. H., & Hunter, J. R. (1974). Fronts in the Irish Sea. *Nature*, 250, 404–406.
- Szekely, T., Marié, L., Arduin, F., Sentchev, A., & Morel, Y. (2012). *Dynamical aspects of the residual circulation in the Iroise Sea*. Continental Shelf Research [in review].
- Szekely, T., Marié, L., Ferron, B., Cambon, G., & Morel, Y. (2012). *Fortnightly variability of a seasonal density front in relation to a tidal residual jet on the continental shelf*. Continental Shelf Research [in review].
- Tokmakian, R., Strub, P. T., & McClean-Padman, J. (1990). Evaluation of the maximum cross-correlation method of estimating sea surface velocities from sequential satellite images. *Journal of Atmospheric and Oceanic Technology*, 7, 852–865.